Published in final edited form as:
J Mol Cell Cardiol. 2014 September ; 74: 115–124. doi:10.1016/j.yjmcc.2014.04.022.

Calmodulin Mutations Associated with Long QT Syndrome Prevent Inactivation of Cardiac L-type Ca^{2+} Currents and Promote Proarrhythmic Behavior in Ventricular Myocytes

Worawan B. Limpitikul[1], **Ivy E. Dick**[1], **Rosy Joshi-Mukherjee**[1], **Michael T. Overgaard**[2], **Alfred L. George Jr.**[3,*], and **David T. Yue**[1]

David T. Yue: dyue@jhmi.edu

[1]Calcium Signals Laboratory, Departments of Biomedical Engineering and Neuroscience, The Johns Hopkins University School of Medicine, Ross Building, Room 713, 720 Rutland Avenue, Baltimore, MD 21205, voice: (410) 955-0078, fax: (410) 955-0549

[2]Department of Biotechnology, Chemistry and Environmental Engineering, Aalborg University, Denmark

[3]Departments of Medicine and Pharmacology, Vanderbilt University, Nashville, TN 37232

Abstract

Recent work has identified missense mutations in calmodulin (CaM) that are associated with severe early-onset long-QT syndrome (LQTS), leading to the proposition that altered CaM function may contribute to the molecular etiology of this subset of LQTS. To date, however, no experimental evidence has established these mutations as directly causative of LQTS substrates, nor have the molecular targets of CaM mutants been identified. Here, therefore, we test whether expression of CaM mutants in adult guinea-pig ventricular myocytes (aGPVM) induces action-potential prolongation, and whether affiliated alterations in the Ca^{2+} regulation of L-type Ca^{2+} channels (LTCC) might contribute to such prolongation. In particular, we first overexpressed CaM mutants in aGPVMs, and observed both increased action potential duration (APD) and heightened Ca^{2+} transients. Next, we demonstrated that all LQTS CaM mutants have the potential to strongly suppress Ca^{2+}/CaM-dependent inactivation (CDI) of LTCCs, whether channels were heterologously expressed in HEK293 cells, or present in native form within myocytes. This attenuation of CDI is predicted to promote action-potential prolongation and boost Ca^{2+} influx. Finally, we demonstrated how a small fraction of LQTS CaM mutants (as in heterozygous patients) would nonetheless suffice to substantially diminish CDI, and derange electrical and Ca^{2+}

Correspondence to: David T. Yue, dyue@jhmi.edu.

*Present address: Department of Pharmacology, Northwestern University Feinberg School of Medicine, Chicago, IL 60611

Disclosures

None.

profiles. In all, these results highlight LTCCs as a molecular locus for understanding and treating CaM-related LQTS in this group of patients.

Keywords

calmodulin; Ca^{2+}/CaM-dependent inactivation (CDI); L-type Ca^{2+} channel; long-QT syndrome; APD prolongation

1. Introduction

Calmodulin (CaM) is a ubiquitous Ca^{2+}-sensor molecule that modulates a vast array of proteins, thereby controlling signaling cascades via Ca^{2+}-dependent adjustment of relevant proteins. As such, CaM critically orchestrates numerous functions, including cellular excitability, muscle contraction, memory, and immunological responses [1, 2]. So important are the functions of CaM that it has long been thought that naturally occurring mutations within this molecule would prove lethal, and that such mutations would thereby play little role in disease processes afflicting living individuals.

Yet, a role for CaM in a number of diseases has begun to emerge. Alterations in the overall level of CaM have been implicated in heart failure [3], schizophrenia [4], and Parkinson's disease [5–7]. Outright CaM mutations in *Drosophila* have been associated with muscle malfunction [8]. Very recently, human genetic studies uncovered *de novo* and heritable CaM mutations (N54I and N98S, start methionine denoted residue 1) that are associated with 11 cases of catecholaminergic polymorphic ventricular tachycardia (CPVT), where altered CaM-ryanodine receptor function is implicated as a major contributing factor [9]. Further, whole-exome and targeted gene sequencing has revealed an association between three *de novo* missense CaM mutations and severe long-QT syndrome (LQTS) with recurrent cardiac arrest [10]. The first hints of underlying mechanism can be gleaned by relating the locations of these mutations to the basic structure-function layout of CaM, a 17 kDa protein comprised of N- and C-terminal lobes linked by a flexible helix. Each lobe of CaM contains two EF hands, canonical Ca^{2+} binding motifs, with the N-lobe having slightly lower Ca^{2+} binding affinity. Ca^{2+} binding to these EF hands induces a conformational change that alters function of target molecules to which CaM is bound, thus transducing changes of intracellular Ca^{2+} concentration [11] into modulation of molecular function. Each of the LQTS mutations (D96V, D130G, and F142L, with start methionine denoted residue 1) resides at or near Ca^{2+} coordinating residues within the EF hands of the C-lobe of CaM, and have been shown to decrease affinity for Ca^{2+} binding [10]. By contrast, the reported CPVT mutations in CaM imparted little-to-mild reduction of Ca^{2+} binding affinity [9]. It is perhaps interesting to speculate that the contrasting effects on Ca^{2+} binding may underlie the elaboration of distinguishable LQTS and CPVT phenotypes by these two classes of mutations. At present, however, the mechanisms linking these mutations in CaM to their corresponding disease phenotypes are essentially unknown.

That said, progress towards elucidating these mechanisms will ultimately prove invaluable in devising personalized therapeutics for afflicted individuals, and in gleaning general lessons about LQTS pathogenesis from these single-point-mutation case examples. Among

the most prominent mechanistic unknowns are the following. First, do the LQTS CaM mutations actually cause the emergence of LQTS substrates in heart? At present, no experimental evidence directly establishes causality. Second, what are the predominant molecular targets through which CaM mutations exert their actions in heart? Likely cardiac myocyte targets abound, including ryanodine receptors (RyR2), voltage-gated Na channels ($Na_V1.5$), slowly activating delayed-rectifier K channels (I_{Ks}), and L-type Ca^{2+} channels [10–12] ($Ca_V1.2$). All of these contribute to shaping action-potential morphology and thereby represent plausible candidates. Third, the severity of the LQTS fits in a seemingly incongruous fashion with the redundancy of human CaM genes (*CALM1*, *CALM2*, and *CALM3*), each of which encodes for an identical CaM molecule at the protein level. Given the heterozygosity of these LQTS patients [10], this redundancy implies that only one of six alleles of CaM would possess a mutation, yielding only a portion of mutant versus wild-type CaM.

Here, therefore, we acutely introduce LQTS CaM mutants into adult guinea-pig ventricular myocytes (aGPVMs) and demonstrate marked prolongation of action potentials, along with intense disturbance of Ca^{2+} cycling. As these effects are reminiscent of those we observed previously by man-made CaM mutants acting strongly through diminished CaM-mediated regulation of L-type Ca^{2+} channels [13] (LTCCs), we tested directly for the effects of naturally occurring LQTS CaM mutants on these very channels. Indeed, we establish that Ca^{2+} regulation of LTCCs can be strongly suppressed by overexpression of LQTS CaM mutants, posturing altered regulation of these channels as an important contributor to the LQTS phenotype. By contrast, overexpressing CPVT CaM mutants caused weaker or undetectable perturbation of LTCC function and action potentials. Finally, we note the requirement that a single Ca^{2+}-free CaM (apoCaM) must first preassociate with LTCCs for subsequent Ca^{2+} regulation to occur [5, 11, 14–17], and substantiate how this feature rationalizes how a limited fraction of LQTS CaM mutants can nonetheless elaborate significant perturbation of channel regulation, sufficient to appreciably prolong action potentials.

2. Methods

2.1 Adult Guinea-pig Ventricular Myocyte Isolation and Adenoviral Transduction

Adult guinea-pig ventricular myocytes (aGPVMs) were isolated from whole hearts of adult guinea pigs (Hartley strain, 3–4 wk old, weight 250–350 g). Hearts were excised after guinea pigs were anesthetized with pentobarbital (35 mg/kg, intraperitoneal injection). Single ventricular myocytes were isolated from both ventricles according to a published protocol [18] and plated on glass coverslips coated with laminin (20 μg/ml overnight at 4 °C). Cells were transduced with adenovirus carrying wild-type or mutant CaM upon plating in the presence of M199 medium supplemented with 20% fetal bovine serum. Expression of wild-type CaM had little effect on action-potential morphology or duration, as compared to uninfected myocytes (Supplementary Figure 1). After 4 hours, the medium was replaced by M199 medium with 0% fetal bovine serum to maintain the phenotype of acutely dissociated myocytes. Cells were maintained at 37 °C and recording was done at room temperature 20–36 hours later.

2.2 Molecular Biology

LQTS CaM mutations were generated using QuikChange ™ site-directed mutagenesis (Agilent) on rat brain CaM (M17069) in the pcDNA3 vector [13] (Invitrogen). CPVT CaM mutations were generated on human *CALM1* gene in the pcDNA3 vector (a kind gift from Michael T. Overgaard [9]). For electrophysiological recordings in HEK293 cells, both wild-type and LQTS mutant CaMs were cloned into the pIRES2-EGFP vector (Clontech Laboratories, Inc.) using *NheI* and *BglII*. For adenoviral expression in aGPVMs, wild-type and mutant CaMs were cloned into the pAdCiG viral shuttle vector using *XhoI* and *SpeI*. Adenovirus was amplified via a standard cre-recombinase method as previously described [13].

The human cardiac α_{1C} cDNA was constructed by cloning in an ~1.6 kbase upstream fragment of the cardiac (containing exon 8a) channel variant (kind gift from Tuck Wah Soong [19]) into a human $\alpha_{1C\text{-}1}$ backbone (NM_000719 kindly gifted from Charlie Cohen of Merck Pharmaceuticals) contained within pcDNA3.1, via *HindIII* and *ClaI* sites.

For FRET two-hybrid constructs, CaM and CI region of $Ca_V1.2$ channels (as defined in Figure 5A and described previously [14]) were tagged on their amino termini with fluorophores (cerulean and venus, respectively) with a linker of 3 alanines, and cloned into the pcDNA3.0 (Invitrogen) using *KpnI* and *XbaI*.

2.3 Transfection of HEK293 Cells

For whole-cell patch clamp experiments, HEK293 cells were cultured on glass coverslips in 10-cm dishes and Ca^{2+} channels were transiently transfected using a standard calcium phosphate method [20]. 8 μg of human cardiac α_{1C} cDNA (as described above) was co-expressed heterologously with 8 μg of rat brain β_{2a} (M80545), 8 μg of rat brain $\alpha_2\delta$ (NM012919.2) subunits, and 8 μg of wild-type or mutant CaMs, except for mixing experiments (Figure 6) where various molar ratios of wild-type to mutant CaM were transfected. The auxiliary β_{2a} subunit was chosen so as to minimize the confounding effects of voltage-dependent inactivation on CDI [21]. To increase expression levels, 2 μg of simian virus 40 T antigen cDNA was co-transfected. Expression of all constructs was driven by a cytomegalovirus promoter.

For FRET two-hybrid experiments, HEK293 cells were cultured on glass-bottom dishes and transfected with polyethylenimine [22] (PEI) before epifluorescence imaging. Whole-cell patch clamp and FRET two-hybrid experiments were performed 1–2 days after transfection.

2.4 Electrophysiology

Whole-cell voltage-clamp recordings of HEK293 cells were done 1–2 days after transfection at room temperature. Recordings were obtained using an Axopatch 200B amplifier (Axon Instruments). Whole-cell voltage-clamp records were lowpass filtered at 2 kHz, and then digitally sampled at 10 kHz. P/8 leak subtraction was used, with series resistances of 1–2 MΩ. For voltage-clamp experiments, internal solutions contained (in mM): $CsMeSO_3$, 114; CsCl, 5; $MgCl_2$, 1; MgATP, 4; HEPES (pH 7.3), 10; and either BAPTA, 10 or EGTA, 1; at 295 mOsm adjusted with $CsMeSO_3$. The free Ca^{2+} concentrations in these BAPTA- and

EGTA-containing were respectively estimated to be ~2.4 and 0.45 pM [23], assuming a contaminant Ca^{2+} concentration of 25 μM (standard conversion at http://maxchelator.stanford.edu/). External solutions contained (in mM): TEA-$MeSO_3$, 140; HEPES (pH 7.4), 10; and $CaCl_2$ or $BaCl_2$, 40; at 300 mOsm, adjusted with TEA-$MeSO_3$. These solutions produced the following uncorrected junction potentials: 10 BAPTA/40 Ca^{2+}: 10.5 mV; 10 BAPTA/40 Ba^{2+}: 10.2 mV; 1 EGTA/40 Ca^{2+}: 11.4 mV; 1 EGTA/40 Ba^{2+}: 11.1 mV [24]. Fraction of peak current remaining after 300-ms depolarization (r_{300}) to various voltages were measured. The extent of Ca^{2+}/CaM-dependent inactivation (CDI) was calculated as $f_{300} = (r_{300/Ba} - r_{300/Ca})/r_{300/Ba}$.

Whole-cell recordings of aGPVMs were performed 20–36 hours post isolation on the same recording setup. Internal solutions for voltage clamp experiments contained, (in mM): $CsMeSO_3$, 114; CsCl, 5; $MgCl_2$, 1; MgATP, 4; HEPES (pH 7.3), 10; BAPTA, 10; and ryanodine, 0.005; at 295 mOsm adjusted with $CsMeSO_3$. External solutions contained (in mM): TEA-$MeSO_3$, 140; HEPES (pH 7.4), 10; and $CaCl_2$ or $BaCl_2$, 5; at 300 mOsm, adjusted with TEA-$MeSO_3$. These solutions produced an 8.4 mV uncorrected junction potential [24]. For current clamp, experiments, internal solutions contained (in mM): K glutamate, 130; KCI, 9; NaCl,10; $MgCl_2$, 0.5; EGTA, 0.5; MgATP, 4; HEPES, 10 (pH 7.3 with KOH). External solution (Tyrode's solution) contained (in mM): NaCl, 135; KCl, 5.4; $CaCl_2$, 1.8; $MgCl_2$, 0.33; NaH_2PO_4, 0.33; HEPES, 5; glucose, 5 (pH 7.4). Junction potentials for current-clamp solutions were calculated to be only 0.5 mV [24]. The time from upstroke to 80% repolarization (APD_{80}) was used as the metric for action potential duration throughout. SD_{cell}, the mean standard deviation of APD_{80} within individual cells, was used to assess the dispersion of APD_{80} at the same expression level of CaM. Throughout, whole-cell voltage-clamp records were lowpass filtered at 2 kHz, and then digitally sampled at 10 kHz. Current-clamp recordings were filtered at 5 kHz, and sampled at 25 kHz.

2.5 Ratiometric Ca^{2+} Imaging

Single aGPVMs were plated on glass-bottom dishes coated with laminin. Cells were loaded with Indo-1 AM (1 μM) at room temperature for 5 minutes, rinsed, and further incubated for 10 minutes in Tyrode's solution at room temperature to allow for de-esterification of Indo-1 AM. Cells were stimulated by application of an electric field across individual cells using a Grass stimulator (SDD9) and bipolar point platinum electrodes. Recordings were made at room temperature in Tyrode's solution supplemented with 10 μM ascorbic acid [25] to buffer free radicals generated from electrical pacing and exposure to UV light. Fluorescence was measured using 340-nm excitation and 405- to 485-nm emission wavelengths. The intracellular Ca^{2+} concentration ($[Ca^{2+}]$) was calculated as $[Ca^{2+}] = K_{d/Indo} \cdot \beta \cdot (R - R_{min})/(R_{max} - R)$. R is the ratio of fluorescence signal at 405 and 485 nm. $K_{d/Indo}$ was determined as 800 nM [26]. R_{min} was determined to be 0.53 in a 0 mM Ca^{2+} Tyrode's with 5 mM EGTA and 1 μM ionomycin. R_{max} was determined to be 2.60 in a Na^+-free Tyrode's (Na^+ was replaced with choline ion to minimize the action of Na-Ca exchanger) with 10 mM Ca^{2+}, 1 μM ionomycin and 10 mM 2,3-butanedione monoxime. β, as defined by the ratio of fluorescence signal at 485 nM under Ca^{2+}-free and Ca^{2+}-bound conditions, was determined to be 2.33. Cells were stimulated with a single electrical pulse after steady-state pacing at

0.1 Hz. The total amount of Ca^{2+} entry was determined by integration of the area under Ca^{2+}-versus-time waveforms. Sarcoplasmic reticulum Ca^{2+} content (SR content) was determined by application of 5 mM caffeine to aGPVMs superfused with a Na^+-free Tyrode's (Na^+ was replaced with choline), containing 1.8 mM Ca^{2+} and 10 mM 2,3-butanedione monoxime. The concentration of caffeine was chosen to minimize Indo-1 quenching [27] but was still sufficient to empty the sarcoplasmic reticulum.

2.6 FRET Two-Hybrid Measurement

Three-cube FRET measurements were performed on HEK293 cells cultured on glass-bottom dishes using an inverted fluorescence microscope in modified Tyrode's solution (in mM, NaCl, 138; KCl, 4; $CaCl_2$, 2; $MgCl_2$, 1; HEPES, 10; glucose, 10). FRET efficiency (E_A) of individual cells was computed based on a published protocol [15]. Differential expression of test constructs across individual cells allowed decoration of a binding curve. Effective dissociation constants ($K_{d,EFF}$) were calculated by fitting the binding curve with the equation $E_A = [D]_{fee}/(K_{d,EEF} + [D]_{free}) \cdot E_{A,max}$, where $[D]_{free}$ is the free concentration of donor molecules.

2.7 Data Analysis and Statistics

All data were analyzed in MATLAB (The MathWorks) using custom-written scripts. For APD_{80} and Ca^{2+} transient measurements the Wilcox rank sum test was used to assess statistical significance of differences between cells expressing wild-type and mutant CaMs. In addition, variability not due to expression differences was assessed by calculating the standard deviation within each cell (SD_{cell}) for both APD_{80} and Ca^{2+} transient measurements. Statistical significance for variability was determined by a student's t-test with the Bonferroni correction for multiple samples as appropriate. Average Ca^{2+} transients are displayed ± SD. Statistical significance for SR content was assessed using a student t-test with a Bonferroni correction for multiple samples. The values are displayed as mean ± SEM. For electrophysiology and FRET two-hybrid measurements, f_{300} and E_A values were expressed as mean ± SEM, and a student's t-test was used to assess statistical significance.

3. Results

3.1 CaM Mutants Promote Proarrhythmic Electrical and Ca^{2+} Activity in Ventricular Myocytes

CaM mutations have been associated with severe LQTS and recurrent cardiac arrest [10], but to date, no direct evidence exists that these mutations can actually promote proarrhythmic properties in an experimental cardiac model. Accordingly, before investigating specific Ca^{2+} regulatory disturbances relating to the interaction of LQTS CaM mutants and individual molecular targets, we tested whether the expression of these mutants at all perturbed the overall electrical and Ca^{2+} cycling properties of aGPVMs. This particular model was chosen because it features action potentials with a prominent plateau phase reminiscent of that in humans, making this system particularly suitable for understanding long-QT phenomena.

Figure 1A displays the prototypic action potentials of a single such myocyte expressing only wild-type CaM (CaM_{WT}), obtained at 0.5-Hz stimulation under whole-cell current clamp. The timing of current injection stimuli is shown underneath for orientation. The waveforms are nearly identical from one stimulus to the next, with a mean action potential duration (APD_{80}) of ~300 ms [13]. Population behavior for APD_{80} is summarized in Figure 1B, which plots the cumulative distribution of durations drawn from 285 responses in 10 cells, where P_{APD} is the probability that APD_{80} is less than the value on the abscissa. The sharp rise of the distribution confirms a mean duration of 349.6 ms, with a modest standard deviation of 79.6 ms. Additionally, the mean standard deviation of APDs within individual myocytes (SD_{cell}, intra-cell standard deviation) was only 21 ms, further indicating relatively homogeneous behavior. By contrast, adenoviral-mediated expression of CaM_{D96V} induced a strikingly different profile (Figure 1C). Here, action potentials could be enormously elongated (red), exceeding even the inter-stimulus interval of 2 seconds. For reference, the control waveform with only CaM_{WT} present is reproduced in gray. Population data, displayed in cumulative histogram format (Figure 1D), reveal marked lengthening and dispersion of APD_{80} values (red), with mean and standard-deviation values of 897.3 and 222.9 ms ($P < 0.001$). Here, SD_{cell} increased to 156.3 ms, indicating significant variability within each cell as compared to CaM_{WT} ($P < 0.01$). Both of these features furnish the cellular substrates for electrically driven arrhythmias at the tissue and organ level [28]. Similar results were obtained for expression of CaM_{D130G} (Figures 1E–F, APD_{80} = 915.3 ± 231.7 msec, $P < 0.001$; SD_{cell} = 78.5 msec, $P \leq 0.01$) and CaM_{F142L} (Figures 1G–H, APD_{80} = 864.9 ± 320.1 msec, $P < 0.001$; SD_{cell} = 179.1 msec, $P < 0.01$). The exemplar for CaM_{D130G} illustrates the occurrence of alternans (Figure 1E), and that for CaM_{F142L} exemplifies simple APD prolongation. All these behaviors (Figures 1C, 1E, 1G) could be observed in the presence of any of the CaM mutants and persist at faster pacing rates (Supplementary Figure 2). Detailed parameters for action potential recordings are in Table 1 and Supplementary Table 1.

Beyond electrical disturbances, Ca^{2+} cycling dysfunction may also drive arrhythmogenesis [29]. Accordingly, we examined the effect of LQTS CaM mutant expression on intracellular Ca^{2+} transients. Figure 1I displays the typical Ca^{2+} waveform in a myocyte expressing only CaM_{WT}. Ratiometric Indo-1 imaging was used to gauge Ca^{2+} activity, and data are shown as the mean ± SD drawn from multiple cells. The black trace plots the mean, and standard deviation bounds are shown by gray shadows. Upon expression of CaM_{D96V}, Ca^{2+} transients are markedly amplified and prolonged (Figure 1J, red). Reproduction of the control CaM_{WT} waveform (gray) serves to emphasize the strong changes in Ca^{2+} activity. Likewise, expression of CaM_{D130G} and CaM_{F142L} produced similarly striking increases of Ca^{2+} transients (Figures 1K–L). Representing these data in cumulative histogram format serves to emphasize the increased dispersion of peak Ca^{2+} transient amplitude produced by CaM mutants (Figures 1M–N). Shown here are the cumulative probabilities of the area under Ca^{2+} transients (P_Q) for CaM_{WT} and CaM mutants as labeled. The precipitous rise of the wild-type distribution confirms the similarity of Ca^{2+} amplitudes among cells (Figure 1M, black relation). By contrast, the sluggish rise of distributions for CaM mutants (Figures 1M and 1N, red relations) reveals marked heterogeneity of Ca^{2+} transients among cells, as confirmed by significantly larger intra-cell standard deviations (gray bars, $P < 0.05$).

Additionally, both diastolic Ca^{2+} concentrations and SR Ca^{2+} content were significantly elevated by overexpressing LQTS CaM mutants (Supplementary Figure 3). In all, CaM mutants furnish the cellular substrates for Ca^{2+}-driven arrhythmias [29], by increasing amplitude and dispersion of Ca^{2+} transients, heightening diastolic Ca^{2+} concentration, and augmenting SR Ca^{2+} content.

3.2 LQTS Calmodulin Mutants Suppress Ca^{2+}/CaM-mediated Inactivation of $Ca_V1.2$ Ca^{2+} Channels

The ability of naturally occurring LQTS CaM mutants to prolong and disperse action potentials was reminiscent of effects we and others observed previously under expression of man-made CaM mutants in the same and similar model systems [13, 30]. There, many of the action potential effects could be attributed to the suppression of a Ca^{2+}/CaM-mediated inactivation (CDI) of $Ca_V1.2$ Ca^{2+} channels. We therefore tested for the effects of the naturally occurring LQTS-related CaM mutants on $Ca_V1.2$ CDI, heterologously expressed in HEK293 cells for maximal biophysical resolution. In this regard, $Ca_V1.2$ expression here included the use of an auxiliary β_{2a} subunit to better visualize CDI effects by minimizing voltage-dependent inactivation [21].

Figure 2A displays exemplar currents of $Ca_V1.2$ channels coexpressed with CaM_{WT}. The sharp decay of Ca^{2+} current (red) evoked by a 30-mV depolarizing step is the well-known result of the CDI process. As confirmation, Ba^{2+} current (black) evoked in the same cell hardly decays, as Ba^{2+} binds poorly to CaM. Population data shown below (Figures 2B–C) rounds out characterization of the baseline behavior of channels in the presence of CaM_{WT}. Figure 2B displays the average of the peak normalized Ba^{2+} current as a function of step potentials, and Figure 2C plots the fraction of peak current remaining after 300-ms depolarization to various voltages (r_{300}). The U-shaped Ca^{2+} r_{300} relation (red) recapitulates the classic hallmark of CDI [31, 32], while the flat $Ba^{2+}r_{300}$ relation (black) confirms the lack of appreciable inactivation without activation of CaM. Hence, the difference between Ba^{2+} and Ca^{2+} r_{300} relations at 30 mV, as normalized by the corresponding Ba^{2+} r_{300} value, formally gauges the extent of CDI ($f_{300} = 0.690 \pm 0.028$).

Upon coexpressing $Ca_V1.2$ channels with mutant CaM_{D96V}, a starkly different functional profile is observed (Figures 2D–F). Here, CDI is strongly suppressed ($f_{300} = -0.009 \pm 0.008$, $P < 0.001$), without shift in the voltage activation profile (Figure 2E). Similarly, coexpression of channels with CaM_{D130G} or CaM_{F142L} also sharply diminished CDI (Figures 2G–I and Figures 2J–L, $f_{300} = -0.002 \pm 0.011$, $P < 0.001$ and 0.065 ± 0.005, $P < 0.001$, respectively). The above results were obtained with strong intracellular Ca^{2+} buffering by 10 mM BAPTA, to restrict Ca^{2+} elevations to those in the nanodomains of individual channels, and thereby minimize cell-to-cell variations owing to differences in current amplitudes. Importantly, however, under more physiological Ca^{2+} buffering (1 mM EGTA) that allows global elevation of Ca^{2+}, strong but incomplete blunting of CDI was produced by the CaM mutants (Supplementary Figure 4). This residual CDI can be attributed to signaling through the N-terminal lobe of CaM (largely unaffected in LQTS CaM mutants), which is sensitive to sustained global elevation of calcium [33, 34]. Overall, the naturally occurring CaM mutants suppressed $Ca_V1.2$ channel CDI, in a manner

indistinguishable from that of a man-made mutant CaM_{34} molecules that selectively eliminate Ca^{2+} binding to the C-but not N-terminal lobe of this molecule [20, 33, 34].

By contrast, overexpressing CPVT CaM mutants had weaker effects on $Ca_V1.2$ channel CDI. CaM_{N54I} yielded no appreciable change in CDI compared to CaM_{WT} (Figures 3A–C, $f_{300} = 0.583 \pm 0.043$, $P > 0.01$). On the other hand, CaM_{N98S} managed only to partially diminish CDI (Figures 3F–H, $f_{300} = 0.367 \pm 0.023$, $P < 0.001$). Both results in Figure 3 were obtained under high Ca^{2+} buffering conditions (10 mM BAPTA). Under more physiological Ca^{2+} buffering (1 mM EGTA), we observed a similar trend wherein CaM_{N54I} and CaM_{N98S} exerted at most modest diminution of CDI (Supplementary Figure 5). To assess further the more integrative consequences of these CDI profiles (Figures 3A–C, F–H), we investigated the effects of these CPVT CaM mutants within aGPVMs. As might be expected, action potentials in the presence of CaM_{N54I} were nearly identical to those with CaM_{WT} (Figures 3D–E). On the other hand, CaM_{N98S} significantly prolonged action potentials (Figures 3I–J, red $P < 0.01$) as compared to CaM_{WT} (gray). Additionally, intra-cell standard deviation (Figure 3J, gray bar) was also larger than CaM_{WT} ($P < 0.05$), positioning CaM_{N98S} for moderate LQTS and affiliated arrhythmias. For CaM_{N54I}, the nearly complete lack of effect on CDI helps explain why this mutation was not associated with LQTS. Interestingly, the intermediate effects of CaM_{N98S} on CDI and action potentials match well with reports of LQTS in an unrelated patient [35].

Thus far, we have demonstrated the ability of the naturally occurring LQTS CaM mutants to markedly attenuate CDI of $Ca_V1.2$ channels heterologously expressed in HEK293 cells, to facilitate biophysical resolution. Nonetheless, we next wondered whether similar effects would be observed in native L-type Ca^{2+} currents, as present in the same aGPVMs as used in Figure 1. Figure 4A displays exemplar L-type currents evoked under whole-cell voltage clamp, using 10 mM BAPTA as the intracellular Ca^{2+} buffer, so as to mimic the condition of Figure 2. Ryanodine (5 μM) was included in the intracellular dialyzate to eliminate phasic Ca^{2+} release from the sarcoplasmic reticulum, and limit CDI to that driven by Ca^{2+} entry through individual L-type Ca^{2+} channels [36]. We again observed strong CDI when Ca^{2+} was used as the charge carrier (red) as compared to a limited amount of voltage-dependent inactivation (VDI) seen in the Ba^{2+} current (black). This additional VDI component is expected in this native setting due to a mix of endogenous beta subunits [37, 38], compared to the pure population of β_{2a} subunits utilized in HEK293 cell experiments. That said, the baseline f_{300} value estimating isolated CDI in control myocytes (Figures 4A–C) was nonetheless 0.67 ± 0.04 (obtained at 20-mV step), which is quite similar to that obtained in recombinant channel expression experiments (Figure 2C). Likewise, population data shows a similar current-voltage relationship and U-shaped Ca^{2+} r_{300} curve (Figures 4B–C). Importantly, expression of mutant CaM_{D96V} essentially abolished CDI in this native setting ($f_{300} = -0.18 \pm 0.03$, $P < 0.001$, Figures 4D–F) and so did CaM_{D130G} and CaM_{F142L} ($f_{300} = 0.02 \pm 0.09$, $P < 0.001$, Figures 4G–I and -0.09 ± 0.03, $P < 0.001$, Figures 4J–L, respectively), supporting a strong mechanistic link between $Ca_V1.2$ channel deficits and the LQTS effects seen in patients carrying the CaM mutations.

3.3 Limited Expression of LQTS CaM Molecules Still Affects $Ca_V1.2$ Channel CDI

We have so far demonstrated that strong overexpression of LQTS-associated CaM molecules in myocytes can produce both strongly dysfunctional electrical and Ca^{2+} cycling, and potently diminished CDI. However, in the actual related patient population, only one of six alleles encodes a mutant CaM, while the other alleles would elaborate wild-type CaM. Accordingly, we would anticipate that only a limited fraction of CaM molecules would bear the pathogenic mutation [10]. How then could the significant cardiac deficits encountered by patients be rationalized? Previous mechanistic studies of L-type channel CDI offer a potential explanation. In particular, it has been shown that for CDI to occur, channels must initially preassociate with a Ca^{2+}-free CaM (apoCaM), to which subsequent Ca^{2+} binding triggers CDI [15, 39]. That is, bulk CaM in the cytoplasm does not appreciably trigger CDI. Thus, if LQTS-associated mutant CaM molecules can still preassociate on par with wild-type CaM, then a sizeable fraction of channels would be bound to mutant CaM, and thus unable to undergo strong CDI (Figures 2–3). Thus, the overall decrease in CDI should be appreciable, reflecting the aggregate fractional presence of mutant CaM in cells.

Accordingly, we utilized a well-established live-cell FRET two-hybrid binding assay to determine whether mutant CaMs can still interact with $Ca_V1.2$, in a manner similar to wild-type CaM. Figure 5A (top) cartoons the relevant sites of apoCaM interaction with $Ca_V1.2$ channels, in particular the CI region of the channel carboxy tail. Our FRET assay therefore paired the $Ca_V1.2$ CI region with CaM (Figure 5A, bottom). As baseline reference, Figure 5B shows the canonical binding curve between the CI region and CaM_{WT}, where this plot displays the acceptor-centric FRET efficiency of interaction (E_A) as a function of the relative free concentration of donor-tagged molecules D_{free} (cerulean-CaM_{WT}). The curve resembles a typical binding reaction, and the D_{free} that produces half-maximal E_A yields an effective dissociation constant ($K_{d,EFF}$) of 12,000 D_{free} units [5]. Reassuringly all three mutant CaM molecules bind at least as well as wild-type CaM (Figures 5B–5E), demonstrating that mixed expression of mutant and wild-type CaM will result in some fraction of channels bound to mutant CaM.

To test this notion quantitatively, we first devised simple means to control the expression ratio of wild-type to mutant CaM molecules ($\hat{\gamma}$) (Supplementary Note 1.6). Then, we performed whole-cell electrophysiology experiments to test explicitly whether the strength of CDI in $Ca_V1.2$ channels would be graded by different $\hat{\gamma}$ values, just as anticipated by the relative binding affinities of channels for mutant versus wild-type apoCaM (Figures 5B–E). Here, our approach was to strongly overexpress variable ratios of such molecules so that the contribution of endogenous CaM would be negligible. If such a scenario were to hold true, we could quantitatively predict that the aggregate CDI strength (*CDI*) as a function of the protein expression ratio of wild-type to mutant CaM, as the Langmuir equation in Figure 6A (Supplementary Note 1.7). CDI_{WT} is the full-strength CDI measured with only wild-type CaM strongly overexpressed, and $K_{d/WT}$ and $K_{d/MUT}$ are the dissociation constants for channel preassociation with wild-type and mutant apoCaM, as specified in Figures 5B–E. Figure 6B plots this relation explicitly as the smooth black curve. Colored data symbols, with corresponding exemplar traces in Figure 6C, nicely decorate this Langmuir function, as do data from numerous other cells (open symbols in Figure 6B). Similar results were

obtained for the other two LQTS-associated CaM mutants (Supplementary Figure 9). Thus, mixtures of wild-type and mutant CaM would weaken L-type channel CDI as predicted by the relative channel affinities for these two molecules in their Ca^{2+}-free form. Based on the relative expression profile of each *CALM* during infancy [10], heterozygous D96V mutation on *CALM2* gene yields $\gamma\tilde{\wedge} 7$, predicting the substantial decrement of CDI indicated by the light rose shading in Figure 6B, likely sufficient to appreciably prolong APDs [30, 40]. Interestingly, the corresponding prediction for a hypothetical homozygous scenario ($\gamma\tilde{\wedge} 3$, dark rose shading) suggests a severe reduction in CDI, potentially incompatible with life. This would perhaps predict the absence of living homozygous individuals.

In all, we would argue that the electrical and calcium dysfunction affiliated with LQTS-associated CaM mutations arises as summarized in Figure 7. Mutant CaM elaborated by a single allele among three *CALM* genes would yield a mixture of wild-type and mutant CaM molecules, as specified by the expression ratio γ. Because channels must first preassociate with apoCaM to undergo subsequent CDI, this fractional expression of mutant CaM would produce graded reduction of overall CDI in myocytes, as demonstrated in Figure 6. This decrement of Ca^{2+} feedback inhibition would elaborate abnormally long action potentials and QT intervals [13], likely in a cell-specific manner dependent on both the precise value of γ, and complex interactions with the configuration of other ion-channel and Ca^{2+}-cycling molecules present. The latter interaction factors likely contribute to the impressive dispersion of properties documented in Figure 1. Given the variable propensity for action potential prolongation and calcium augmentation within different cells, arrhythmogenic behavior at the tissue and organ level could thus result. Although other effects of mutant CaM molecules are likely to contribute to overall pathogenesis (Figure 7, gray pathway with arrow), this study furnishes strong evidence that a major underlying mechanism concerns the attenuation of L-type calcium channel CDI by the presence of LQTS-associated mutant CaM molecules. This outcome furnishes at least one major molecular target that merits scrutiny for potential therapeutics.

4. Discussion

Our experiments demonstrate that CaM bearing LQTS mutations induce the cellular substrates that would favor a LQTS phenotype. Acute introduction of LQTS mutant CaMs into aGPVMs lead to: (1) electrical disturbances including prolonged APD and electrical alternans, as well as (2) Ca^{2+} cycling disturbances, such as increased Ca^{2+} transients and SR Ca^{2+} load. Importantly, such alterations manifested in a highly dispersed fashion across and within cells, thus furnishing a critical ingredient for arrhythmogenesis at the tissue and organ levels [28]. The present study also clearly indicates that a key contributor to these effects involves the disruption of L-type channel CDI by LQTS CaM mutants. Such CDI attenuation would elaborate increased Ca^{2+} current during phases 2 and 3 of the action potentials, thus prolonging APD and increasing SR Ca^{2+} load. Finally, we have established one scenario by which a small fraction of CaM mutants would suffice to create an appreciable prolongation of action potentials. Preassociation of apoCaM to the $Ca_V1.2$ channels plays a critical role, enabling a fraction of channels to be occupied by the CaM mutants with resulting failure to undergo CDI.

Interestingly, CaM mutants commonly affiliated with CPVT exhibited negligible or weaker effects on action potential duration and L-type channel CDI. The complete lack of effect of CaM_{N54I} on CDI and action potential duration is well explained by its near wild-type Ca^{2+} binding affinity [41], and these molecular and cellular outcomes fit nicely with the lack of appreciable QT prolongation in corresponding probands [9]. This CPVT-associated mutant could nonetheless interact with other targets like RyR2 calcium release channels to potentially contribute to pathogenesis [41]. On the other hand, the CPVT CaM mutant N98S is capable of producing either CPVT [9, 41] or LQTS in patients [35]. This dual effect may well arise from the overlapping effects of these mutations on multiple CaM targets in the heart. Indeed, CaM_{N98S} turned out to both reduce L-type channel CDI and moderately prolong cardiac action potentials (Figure 3). The intermediate effects of this CaM mutant thus rationalize how LQTS or CPVT may become the more prominent clinical phenotype, perhaps as a function of differing expression levels among patients.

In addition to L-type ($Ca_V1.2$) channels, other molecular targets of CaM remain as potential contributors to LQTS pathogenesis. Focusing in particular on targets that preassociate with Ca^{2+}-free CaM, voltage-gated Na channels [42] ($Na_V1.5$) and slow delayed rectifier K channels [43] (I_{Ks}) loom among likely targets. In $Na_V1.5$ channels, Ca^{2+}/CaM is proposed to both facilitate initial opening and stabilize the inactivated state [42]. However, a recent study reports that LQTS CaM mutants lacked significant effects on most splice variants of $Na_V1.5$ channels, though the CaM_{D130G} mutant appeared to moderately enhance persistent current in one fetal splice variant [44]. For I_{Ks}, Ca^{2+}-free CaM may help traffic channels to plasmalemma [45], and Ca^{2+}/CaM is believed to facilitate opening. In fact, mutations in I_{Ks} that disrupt CaM binding result in decreased K current, thus causing LQTS [43, 46]. More broadly, because CaM regulates many other Ca^{2+} channel subtypes, including those predominate in neurons and immune cells, disruption of CDI could lead to a multi-system disorder similar to Timothy syndrome [47–49]. It may well be that extra-cardiac effects are also present in patients possessing LQTS CaM mutants, but that these effects were not recognized in the face of immediately life-threatening cardiac-related sequelae. For other CaM-modulated signaling molecules that do not preassociate with Ca^{2+}-free CaM, the present study would suggest that a limited fraction of LQTS CaM mutants would matter little. Only when the fraction of CaM mutants approaches unity would this class of targets be predicted to exhibit altered function. Key members of this class of CaM targets in cardiac myocytes would include Ca^{2+}/CaM-dependent kinase II (CaMKII) and calcineurin (CN). CaMKII has been argued to influence the electrical properties of cardiomyocytes by phosphorylation of ryanodine receptors, phospholamban, SERCA, and L-type Ca^{2+} channels, all of which could alter electrical and Ca^{2+} function [50]. By contrast, the Ca^{2+}/CaM-activated phosphatase CN dephosphorylates numerous targets including the transcription factor NFAT, implicated in regulating expression levels of numerous ion channels in heart [51]. Nonetheless, if our insights are correct regarding the necessary role of target preassociation with apoCaM to amplify the effects of a limited fraction of CaM mutants, molecules like CaMKII and CN may play little role in the LQTS phenotype at hand.

Even before testing for a role of the additional target molecules alluded to above, potential targeted therapeutic strategies in patients expressing LQTS CaM mutants are suggested by

our finding that LTCC dysfunction likely contributes in this particular setting. In addition to beta-adrenergic blockade, as per the general standard of care for LQTS patients, immediate benefits may arise by seeking appropriate modulators of LTCCs such as roscovitine, which has demonstrated beneficial effects within certain *in vitro* models of LTCC-related LQTS [52]. Additionally, a recent study implicates a non-linear threshold effect between the extent of CDI diminution in LTCCs and onset of outright arrhythmias [53], rather than a continuously graded interrelation. Accordingly, only a few-fold decrease in the fraction of CaM mutants ($\hat{\gamma}$) may yield marked improvement of electrical stability and decrease in the incidence of cardiac arrest. The limited alteration of $\hat{\gamma}$ potentially required to bring about these benefits may considerably improve the feasibility of devising novel therapies towards this end.

Although the prevalence of diseases caused by *de novo* CaM mutations is limited, investigating their pathogenesis may offer revealing opportunities to expand our basic knowledge of LQTS-related arrhythmogenesis. Moreover, additional discoveries of CaM mutations will help expand our database of related genotype-phenotype correlations, lending further resources for understanding. Indeed, following the first discoveries of CaM mutations, three more recent preliminary studies [35, 54, 55] have uncovered further CaM-affiliated arrhythmias. These include the following, listed according to gene and syndrome: D134H (*CALM2*; LQTS), N98S (*CALM2*; LQTS), D132F (*CALM2*; LQTS and CPVT), N54I (*CALM1*; LQTS and/or sudden unexplained death in the young (SUDY)), A103V (*CALM3*; CPVT and/or SUDY), F90L (*CALM1*; ventricular fibrillation). These exciting discoveries suggest that a small yet substantial population of patients with CaM mutations is emerging, thus necessitating the inclusion of *CALM* genes in genetic test panels for LQTS and CPVT, and providing added motivation for the discovery of new therapies. In this light, it may be warranted to dub this expanding group of CaM-related disorders as calmodulinopathies.

Supplementary Material

Refer to Web version on PubMed Central for supplementary material.

Acknowledgments

We would like to thank Philemon Yang and Wanjun Yang with their help in adenovirus amplification, and Manu Ben Johny for advice on optimizing FRET two-hybrid assays of apoCaM with the CI region of $Ca_V1.2$ channels, and initial electrophysiological characterization of CPVT CaM mutants.

Sources of Funding

This research was supported by the Predoctoral Fellowship from the American Heart Association (W.B.L.); R37HL076795 MERIT (D.T.Y.); and R01HL083374 (A.L.G.).

Nonstandard Abbreviations and Acronyms

CaM	calmodulin
CPVT	catecholaminergic polymorphic ventricular tachycardia

LQT(S)	long-QT (syndrome)
aGPVM(s)	adult guinea-pig ventricular myocyte(s)
LTCC(s)	L-type Ca^{2+} channels
apoCaM	Ca^{2+}-free calmodulin
APD	action potential duration
CDI	Ca^{2+}/CaM-dependent inactivation

References

1. Pitt GS. Calmodulin and CaMKII as molecular switches for cardiac ion channels. Cardiovasc Res. 2007; 73:641–7. [PubMed: 17137569]
2. Hoeflich KP, Ikura M. Calmodulin in action: diversity in target recognition and activation mechanisms. Cell. 2002; 108:739–42. [PubMed: 11955428]
3. Ikeda S, He A, Kong SW, Lu J, Bejar R, Bodyak N, et al. MicroRNA-1 negatively regulates expression of the hypertrophy-associated calmodulin and Mef2a genes. Mol Cell Biol. 2009; 29:2193–204. [PubMed: 19188439]
4. Chambers JS, Thomas D, Saland L, Neve RL, Perrone-Bizzozero NI. Growth-associated protein 43 (GAP-43) and synaptophysin alterations in the dentate gyrus of patients with schizophrenia. Prog Neuropsychopharmacol Biol Psychiatry. 2005; 29:283–90. [PubMed: 15694236]
5. Bazzazi H, Ben Johny M, Adams PJ, Soong TW, Yue DT. Continuously Tunable Ca(2+) Regulation of RNA-Edited CaV1.3 Channels. Cell Rep. 2013; 5:367–77. [PubMed: 24120865]
6. Lee D, Lee SY, Lee EN, Chang CS, Paik SR. alpha-Synuclein exhibits competitive interaction between calmodulin and synthetic membranes. J Neurochem. 2002; 82:1007–17. [PubMed: 12358748]
7. Chan CS, Guzman JN, Ilijic E, Mercer JN, Rick C, Tkatch T, et al. 'Rejuvenation' protects neurons in mouse models of Parkinson's disease. Nature. 2007; 447:1081–6. [PubMed: 17558391]
8. Wang B, Sullivan KM, Beckingham K. Drosophila calmodulin mutants with specific defects in the musculature or in the nervous system. Genetics. 2003; 165:1255–68. [PubMed: 14668380]
9. Nyegaard M, Overgaard MT, Sondergaard MT, Vranas M, Behr ER, Hildebrandt LL, et al. Mutations in calmodulin cause ventricular tachycardia and sudden cardiac death. Am J Hum Genet. 2012; 91:703–12. [PubMed: 23040497]
10. Crotti L, Johnson CN, Graf E, De Ferrari GM, Cuneo BF, Ovadia M, et al. Calmodulin mutations associated with recurrent cardiac arrest in infants. Circulation. 2013; 127:1009–17. [PubMed: 23388215]
11. Mori MX, Erickson MG, Yue DT. Functional stoichiometry and local enrichment of calmodulin interacting with Ca2+ channels. Science. 2004; 304:432–5. [PubMed: 15087548]
12. Saucerman JJ, Bers DM. Calmodulin binding proteins provide domains of local Ca2+ signaling in cardiac myocytes. J Mol Cell Cardiol. 2012; 52:312–6. [PubMed: 21708171]
13. Alseikhan BA, DeMaria CD, Colecraft HM, Yue DT. Engineered calmodulins reveal the unexpected eminence of Ca2+ channel inactivation in controlling heart excitation. Proc Natl Acad Sci U S A. 2002; 99:17185–90. [PubMed: 12486220]
14. Ben Johny M, Yang PS, Bazzazi H, Yue DT. Dynamic switching of calmodulin interactions underlies Ca2+ regulation of CaV1.3 channels. Nat Commun. 2013; 4:1717. [PubMed: 23591884]
15. Erickson MG, Alseikhan BA, Peterson BZ, Yue DT. Preassociation of calmodulin with voltagegated Ca(2+) channels revealed by FRET in single living cells. Neuron. 2001; 31:973–85. [PubMed: 11580897]
16. Liu X, Yang PS, Yang W, Yue DT. Enzyme-inhibitor-like tuning of Ca(2+) channel connectivity with calmodulin. Nature. 2010; 463:968–72. [PubMed: 20139964]

17. Pitt GS, Zuhlke RD, Hudmon A, Schulman H, Reuter H, Tsien RW. Molecular basis of calmodulin tethering and Ca2+-dependent inactivation of L-type Ca2+ channels. J Biol Chem. 2001; 276:30794–802. [PubMed: 11408490]
18. Joshi-Mukherjee R, Dick IE, Liu T, O'Rourke B, Yue DT, Tung L. Structural and functional plasticity in long-term cultures of adult ventricular myocytes. J Mol Cell Cardiol. 2013; 65C:76–87. [PubMed: 24076394]
19. Tang ZZ, Liang MC, Lu S, Yu D, Yu CY, Yue DT, et al. Transcript scanning reveals novel and extensive splice variations in human l-type voltage-gated calcium channel, Cav1.2 alpha1 subunit. J Biol Chem. 2004; 279:44335–43. [PubMed: 15299022]
20. Peterson BZ, DeMaria CD, Adelman JP, Yue DT. Calmodulin is the Ca2+ sensor for Ca2+-dependent inactivation of L-type calcium channels. Neuron. 1999; 22:549–58. [PubMed: 10197534]
21. Dafi O, Berrou L, Dodier Y, Raybaud A, Sauve R, Parent L. Negatively charged residues in the N-terminal of the AID helix confer slow voltage dependent inactivation gating to CaV1.2. Biophys J. 2004; 87:3181–92. [PubMed: 15339810]
22. Lambert RC, Maulet Y, Dupont JL, Mykita S, Craig P, Volsen S, et al. Polyethylenimine-mediated DNA transfection of peripheral and central neurons in primary culture: probing Ca2+ channel structure and function with antisense oligonucleotides. Mol Cell Neurosci. 1996; 7:239–46. [PubMed: 8726106]
23. Bers DM, Patton CW, Nuccitelli R. A practical guide to the preparation of Ca(2+) buffers. Methods Cell Biol. 2010; 99:1–26. [PubMed: 21035681]
24. Barry PH. JPCalc, a software package for calculating liquid junction potential corrections in patch-clamp, intracellular, epithelial and bilayer measurements and for correcting junction potential measurements. J Neurosci Methods. 1994; 51:107–16. [PubMed: 8189746]
25. Sathaye A, Bursac N, Sheehy S, Tung L. Electrical pacing counteracts intrinsic shortening of action potential duration of neonatal rat ventricular cells in culture. J Mol Cell Cardiol. 2006; 41:633–41. [PubMed: 16950369]
26. Bassani JW, Bassani RA, Bers DM. Calibration of indo-1 and resting intracellular [Ca]i in intact rabbit cardiac myocytes. Biophys J. 1995; 68:1453–60. [PubMed: 7787031]
27. McKemy DD, Welch W, Airey JA, Sutko JL. Concentrations of caffeine greater than 20 mM increase the indo-1 fluorescence ratio in a Ca(2+)-independent manner. Cell Calcium. 2000; 27:117–24. [PubMed: 10756978]
28. Arevalo H, Rodriguez B, Trayanova N. Arrhythmogenesis in the heart: Multiscale modeling of the effects of defibrillation shocks and the role of electrophysiological heterogeneity. Chaos. 2007; 17:015103. [PubMed: 17411260]
29. Xie LH, Weiss JN. Arrhythmogenic consequences of intracellular calcium waves. Am J Physiol Heart Circ Physiol. 2009; 297:H997–H1002. [PubMed: 19561309]
30. Mahajan A, Sato D, Shiferaw Y, Baher A, Xie LH, Peralta R, et al. Modifying L-type calcium current kinetics: consequences for cardiac excitation and arrhythmia dynamics. Biophys J. 2008; 94:411–23. [PubMed: 18160661]
31. Brehm P, Eckert R. Calcium entry leads to inactivation of calcium channel in Paramecium. Science. 1978; 202:1203–6. [PubMed: 103199]
32. Brehm P, Eckert R, Tillotson D. Calcium-mediated inactivation of calcium current in Paramecium. J Physiol. 1980; 306:193–203. [PubMed: 6257894]
33. Dick IE, Tadross MR, Liang H, Tay LH, Yang W, Yue DT. A modular switch for spatial Ca2+ selectivity in the calmodulin regulation of CaV channels. Nature. 2008; 451:830–4. [PubMed: 18235447]
34. Tadross MR, Dick IE, Yue DT. Mechanism of local and global Ca2+ sensing by calmodulin in complex with a Ca2+ channel. Cell. 2008; 133:1228–40. [PubMed: 18585356]
35. Makita N, Yagihara N, Crotti L, Johnson CN, Beckermann B-M, Shigemizu D, et al. Abstract 13371: CALM2 Mutations Associated With Atypical Juvenile Long QT Syndrome. Circulation. 2013; 128:A13371.
36. Grandi E, Morotti S, Ginsburg KS, Severi S, Bers DM. Interplay of voltage and Ca-dependent inactivation of L-type Ca current. Prog Biophys Mol Biol. 2010; 103:44–50. [PubMed: 20184915]

37. Hullin R, Singer-Lahat D, Freichel M, Biel M, Dascal N, Hofmann F, et al. Calcium channel beta subunit heterogeneity: functional expression of cloned cDNA from heart, aorta and brain. EMBO J. 1992; 11:885–90. [PubMed: 1312465]
38. Olcese R, Qin N, Schneider T, Neely A, Wei X, Stefani E, et al. The amino terminus of a calcium channel beta subunit sets rates of channel inactivation independently of the subunit's effect on activation. Neuron. 1994; 13:1433–8. [PubMed: 7993634]
39. Zuhlke RD, Pitt GS, Deisseroth K, Tsien RW, Reuter H. Calmodulin supports both inactivation and facilitation of L-type calcium channels. Nature. 1999; 399:159–62. [PubMed: 10335846]
40. Morotti S, Grandi E, Summa A, Ginsburg KS, Bers DM. Theoretical study of L-type Ca(2+) current inactivation kinetics during action potential repolarization and early afterdepolarizations. J Physiol. 2012; 590:4465–81. [PubMed: 22586219]
41. Hwang HS, Nitu FR, Yang Y, Walweel K, Pereira L, Johnson CN, et al. Divergent regulation of ryanodine receptor 2 calcium release channels by arrhythmogenic human calmodulin missense mutants. Circ Res. 2014; 114:1114–24. [PubMed: 24563457]
42. Van Petegem F, Lobo PA, Ahern CA. Seeing the forest through the trees: towards a unified view on physiological calcium regulation of voltage-gated sodium channels. Biophys J. 2012; 103:2243–51. [PubMed: 23283222]
43. Shamgar L, Ma L, Schmitt N, Haitin Y, Peretz A, Wiener R, et al. Calmodulin is essential for cardiac IKS channel gating and assembly: impaired function in long-QT mutations. Circ Res. 2006; 98:1055–63. [PubMed: 16556865]
44. Murphy LL, Campbell CM, Crotti L, Johnson CN, Kunic JD, Schwartz PJ, et al. Abstract 14999: Calmodulin Mutation Associated With Neonatal Long-QT Syndrome Evokes Increased Persistent Sodium Current From a Fetal Nav1.5 Splice Variant. Circulation. 2013; 128:A14999.
45. Roden DM. A new role for calmodulin in ion channel biology. Circ Res. 2006; 98:979–81. [PubMed: 16645144]
46. Ghosh S, Nunziato DA, Pitt GS. KCNQ1 assembly and function is blocked by long-QT syndrome mutations that disrupt interaction with calmodulin. Circ Res. 2006; 98:1048–54. [PubMed: 16556866]
47. Raybaud A, Dodier Y, Bissonnette P, Simoes M, Bichet DG, Sauve R, et al. The role of the GX9GX3G motif in the gating of high voltage-activated Ca2+ channels. J Biol Chem. 2006; 281:39424–36. [PubMed: 17038321]
48. Splawski I, Timothy KW, Decher N, Kumar P, Sachse FB, Beggs AH, et al. Severe arrhythmia disorder caused by cardiac L-type calcium channel mutations. Proc Natl Acad Sci U S A. 2005; 102:8089–96. discussion 6–8. [PubMed: 15863612]
49. Splawski I, Timothy KW, Sharpe LM, Decher N, Kumar P, Bloise R, et al. Ca(V)1.2 calcium channel dysfunction causes a multisystem disorder including arrhythmia and autism. Cell. 2004; 119:19–31. [PubMed: 15454078]
50. Rokita AG, Anderson ME. New therapeutic targets in cardiology: arrhythmias and Ca2+/calmodulin-dependent kinase II (CaMKII). Circulation. 2012; 126:2125–39. [PubMed: 23091085]
51. Eder P, Molkentin JD. TRPC channels as effectors of cardiac hypertrophy. Circ Res. 2011; 108:265–72. [PubMed: 21252153]
52. Yazawa M, Hsueh B, Jia X, Pasca AM, Bernstein JA, Hallmayer J, et al. Using induced pluripotent stem cells to investigate cardiac phenotypes in Timothy syndrome. Nature. 2011; 471:230–4. [PubMed: 21307850]
53. Dick, IE.; Joshi-Mukherjee, R.; Yue, DT. Biophysical Society. San Diego: Biophysical Journal; 2012. Nonlinear behavior in the induction of arrhythmias by channels bearing Timothy Syndrome mutations; p. 542a
54. Boczek NJ, Will ML, Loporcaro CG, Tester DJ, Ackerman MJ. Abstract 14699: Spectrum and Prevalence of CALM1, CALM2, and CALM3 Mutations in Long QT Syndrome, Catecholaminergic Polymorphic Ventricular Tachycardia, Idiopathic Ventricular Fibrillation, and Sudden Unexplained Death in the Young. Circulation. 2013; 128:A14699.
55. Marsman RF, Barc J, Beekman L, Alders M, Dooijes D, van den Wijngaard A, et al. A mutation in CALM1 encoding calmodulin in familial idiopathic ventricular fibrillation in childhood and adolescence. J Am Coll Cardiol. 2013

56. Busch AE, Suessbrich H, Waldegger S, Sailer E, Greger R, Lang H, et al. Inhibition of IKs in guinea pig cardiac myocytes and guinea pig IsK channels by the chromanol 293B. Pflugers Arch. 1996; 432:1094–6. [PubMed: 8781206]

57. Mitcheson JS, Hancox JC, Levi AJ. Action potentials, ion channel currents and transverse tubule density in adult rabbit ventricular myocytes maintained for 6 days in cell culture. Pflugers Arch. 1996; 431:814–27. [PubMed: 8927497]

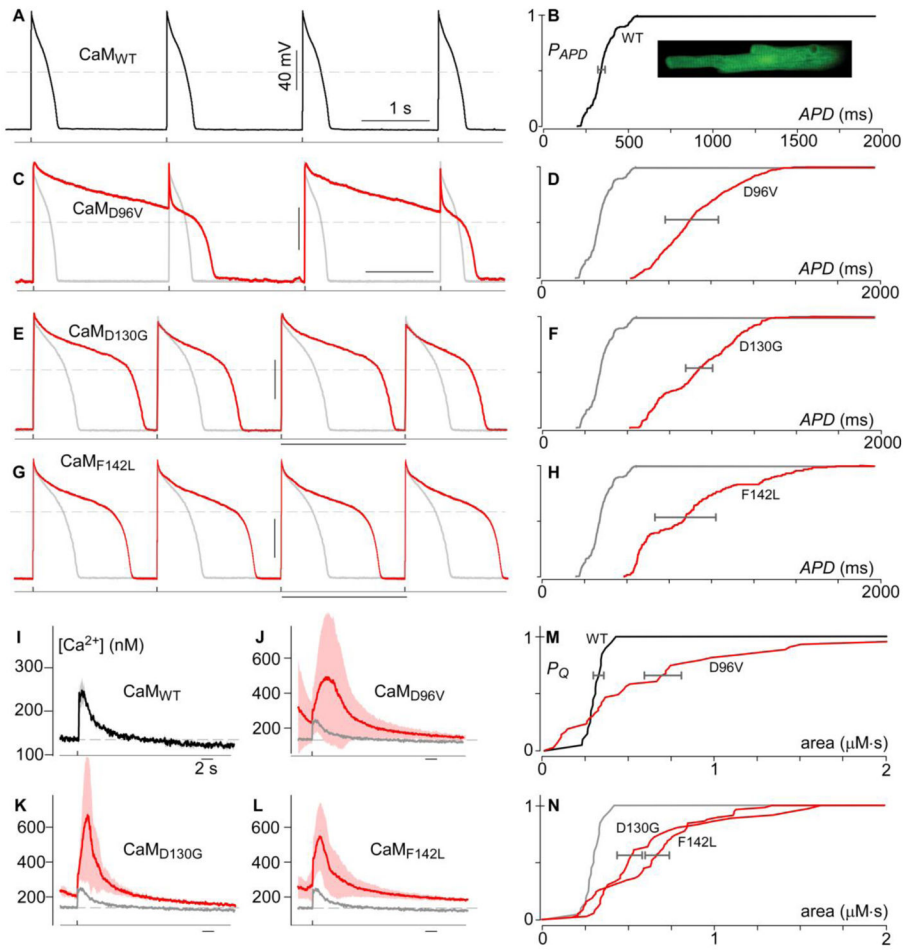

Figure 1. CaM mutants induce arrhythmia

A, Exemplar action potentials recorded via current clamp from one-day-old aGPVMs transduced with CaM_{WT}. The stimulus waveform is depicted below. The dashed horizontal gray line indicates 0 mV, here and throughout.

B, Population data corresponding to **A** plotted as the cumulative distribution of APD_{80} (285 responses from 10 cells). All APD_{80} population data in panels **B**, **D**, **F**, and **H** from myocytes stimulated at 0.5 Hz. Gray bar in **B** displays SD_{cell}. Inset shows confocal image of typical myocyte expressing GFP as a marker of transduction by adenoviral CaM_{WT}.

C, Transduction of the mutant CaM_{D96V} induced marked prolongation of action potentials in this exemplar recording (red) as compared to CaM_{WT} transduction (gray, reproduced from **A**).

D, The cumulative distribution for APD_{80} from CaM_{D96V} transduced aGPVMs (red) demonstrates a dramatic increase in APD_{80} and much greater APD_{80} variability (gray bar, $P \leq 0.01$), both as compared to myocytes transduced with CaM_{WT}.

E–H, Similar AP disturbances were induced via transduction of CaM_{D130G} (**E, F**) and CaM_{F142L} (**G, H**). Example of electrical alternans in aGPVM expressing CaM_{D130G} (**E**). Data displayed in **E** and **G** were obtained during pacing at 1 Hz.

I, Average Ca^{2+} transient (black) recorded from aGPVMs transduced with CaM_{WT} after steady-state pacing at 0.1 Hz, n =5 cells. Standard deviation range shown as gray shading. Indo-1 AM was used as the inorganic Ca^{2+}-sensitive fluorescent dye.

J–L, Transduction of mutant CaMs resulted in dramatic increases in the amplitude and variability of the Ca^{2+} transients. Solid gray trace reproduces the CaM_{WT} data for reference, while red and rose depict average and standard deviation of Ca^{2+} transients from aGPVMs expressing the three mutants as labeled. Data averaged from n = 11, 9, and 15 myocytes for respective panels **J–L.**

M, Population data for CaM_{WT} (black) and CaM_{D96V} (red), plotted as cumulative histograms for the area integrated under the Ca^{2+} transient waveform recorded from each myocyte. Horizontal error bars depict average standard deviation of Ca^{2+} entry for transients within the same cells, and is significantly larger for each LQTS CaM mutant ($P < 0.05$). The significant right shift due to transduction of CaM_{D96V} demonstrates a remarkable increase in Ca^{2+} entry during single APs, while the slower rise indicates greater heterogeneity across myocytes transduced with CaM mutants.

N, Cumulative histograms of Ca^{2+} entry for CaM_{D130G} (red, left) and CaM_{F142L} (red, right), with the fit for CaM_{WT} reproduced in gray.

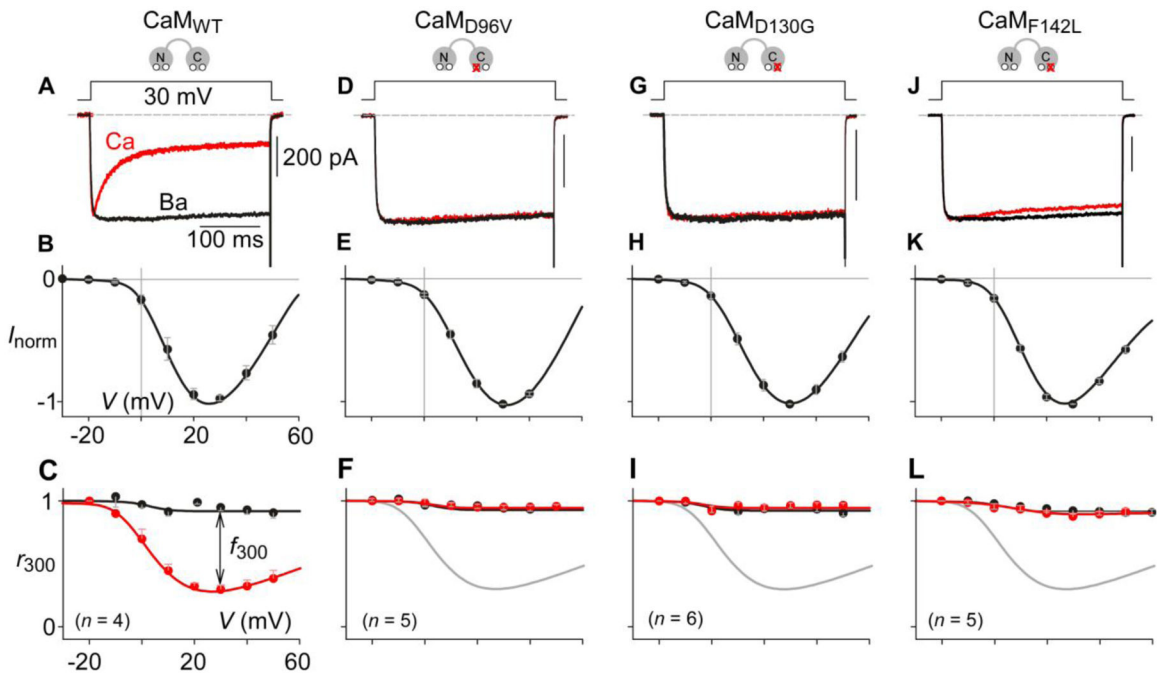

Figure 2. LQTS CaM mutants diminish CDI in HEK293 cells

A, Exemplar currents evoked by 30-mV voltage step (top) in cells co-transfected with $Ca_V1.2$ and CaM_{WT}. CDI manifests as the stronger decay in Ca^{2+} (red) current as compared to Ba^{2+} (black). Ba^{2+} trace is scaled downward to match the peak of the Ca^{2+} trace, thus facilitating comparison of decay kinetics, and the scale bar for current references the Ca^{2+} trace, here and throughout.

B, Average normalized peak current versus voltage relation obtained with Ba^{2+} for the same cells as in **A**. Data are plotted as mean ± SEM here and throughout.

C, Population data for CDI across voltages. r_{300} measures the current remaining after 300 ms, after normalization to peak current. f_{300} is the difference between Ca^{2+} and Ba^{2+} at 30 mV, after normalization by the Ba^{2+} r_{300} value.

D, Expression of CaM_{D96V} severely blunts CDI of $Ca_V1.2$.

E, The current-voltage relation for the CaM_{D96V} scenario remains unaltered.

F, Population data bears out the CaM_{D96V} reduction of CDI across voltages. For reference, the Ca^{2+} r_{300} curve for CaM_{WT} is reproduced in gray.

G–L, CaM_{D130G} and CaMF142L also induce dramatic CDI deficits. Format as in **D–F**.

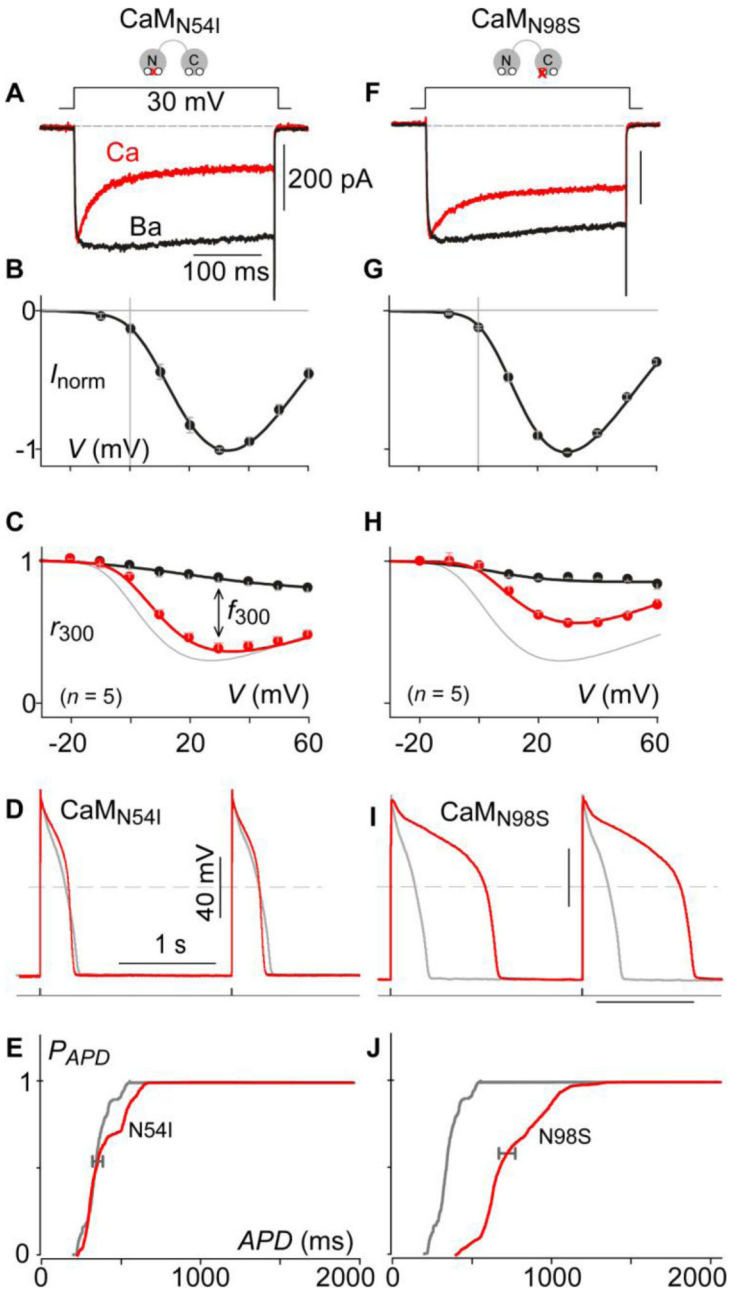

Figure 3. CPVT CaM mutants exert weaker effects on CDI

A, Exemplar currents evoked by 30-mV voltage step (top) in HEK293 cells co-transfected with $Ca_V1.2$ and CaM_{N54I}. Here, coexpression of CaM_{N54I} did not disrupt CDI compared to CaM_{WT} (Figure 2A).

B, Average normalized peak current-voltage relationship for same cells as in **A.** Compared to CaM_{WT} (Figure 2B), there is no shift in voltage activation.

C, Voltage dependence of r_{300} values for Ca^{2+} (red) and Ba^{2+} (black). Ca^{2+} relation for CaM_{WT} configuration reproduced in gray for reference. No significant alteration of CDI across all test voltages.

D-**E**, Coexpression of CaM_{N54I} does not appreciably effect action potentials (red) as compared to co-expression of CaM_{WT} (gray). Format as in Figure 1. Data for panel **E** from 679 action potentials drawn from 6 myocytes.

F, Expression of CaM_{N98S}, however, modestly diminishes CDI, without affecting voltage activation (**G**).

H, Population data of r_{300} values confirm a small, but significant reduction of CDI across voltages.

I-**J**, Overexpression of CaM_{N98S} has the ability to lengthen and increase heterogeneity of action potentials ($P < 0.01$). Format as in Figure 1B. Horizontal error bars in panels **E** and **J** display standard deviation of APD_{80} within cells. Data for panel **J** from 1100 action potentials drawn from 6 myocytes.

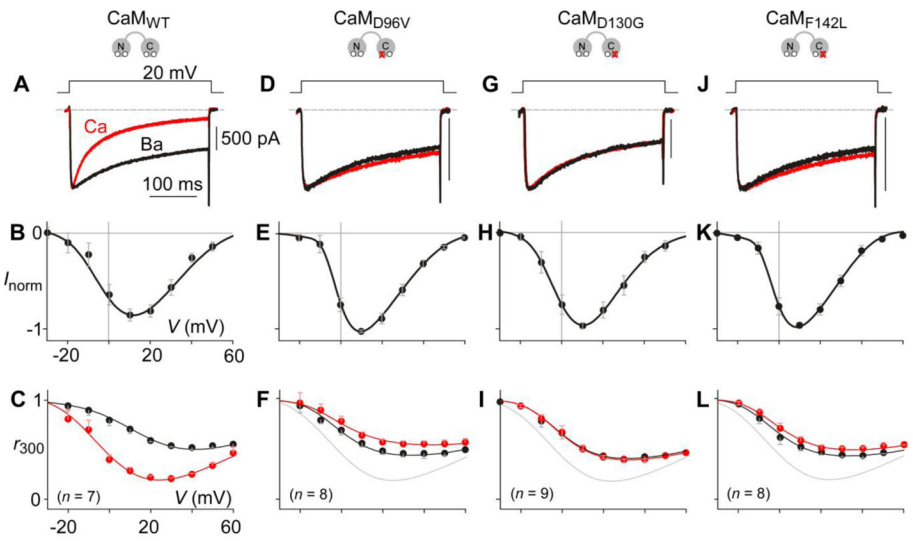

Figure 4. CaM mutants diminish CDI in aGPVMs

A, CDI in native LTCCs recorded from one-day-old aGPVMs transduced with CaM_{WT}. Exemplar current traces elicited by a 20-mV voltage step (top) display strong CDI with Ca^{2+} (red), and a small amount VDI with Ba^{2+} (black).

B, Average normalized peak current-voltage relation obtained in Ba^{2+} for the same cells as in **A**

C, Population data for CDI across voltages. f_{300} is measured at 20 mV.

D, Expression of CaM_{D96V} severely blunts CDI in the native setting.

E, Current-voltage relation in the presence of CaM_{D96V} remains unaltered.

F, Population data confirms the CaM_{D96V} reduction of CDI across voltages. For reference, the Ca^{2+} r_{300} curve for CaM_{WT} is reproduced in gray.

G–L, CaM_{D130G} and CaM_{F142L} also induce dramatic CDI deficits. Format as in **D**-**F**.

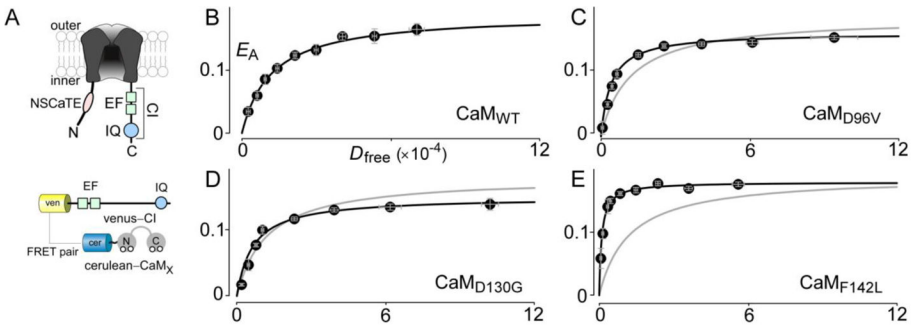

Figure 5. Mutant CaMs bind to Ca$_V$1.2 channels at least as well as wild-type CaM

A, Cartoon depicting CaM interaction domains on the Ca$_V$1.2 calcium channel (CI segment). Below, construct schematics depicting FRET interaction pairs used for binding assessment.

B, The canonical FRET binding curve between the CI region and CaM$_{WT}$. In particular, an acceptor-centric FRET efficiency (E_A) is plotted as a function of the relative free concentration of donor-tagged molecules D_{free} (cerulean-CaM$_{WT}$). $K_{d/EFF}$ for CaM$_{WT}$ binding to CI region is 12000 D_{free} units [5].

C-**E**, FRET binding curves between the CI region and CaM$_{D96V}$ (**C**), CaM$_{D130G}$ (**D**) and CaM$_{F142L}$ (**E**). $K_{d/EFF}$ are 4000, 6500, and 1000 D_{free} units, respectively. The binding curve for CaM$_{WT}$ is reproduced in gray for reference.

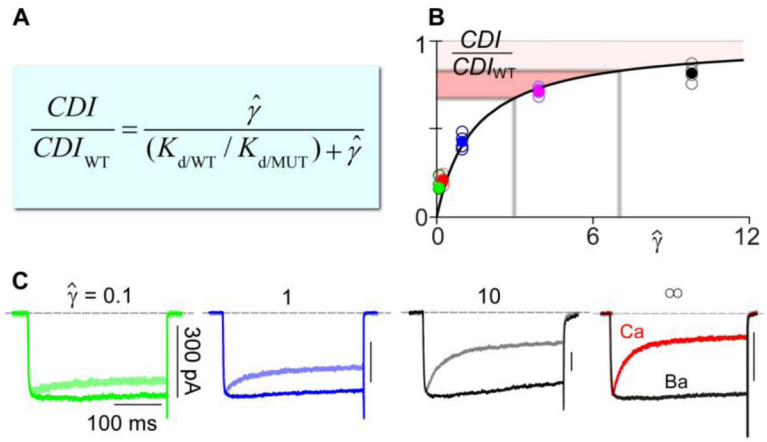

Figure 6. Dose-dependent effect of mutant CaMs

A, Langmuir equation relating the extent of CDI and wild-type versus mutant CaM expression ratio $\hat{\gamma}$.

B, Predicted CDI as a function of $\hat{\gamma}$ (black). Solid circles indicate average data for each ratio $\hat{\gamma}$; open circles pertain to data for individual cells. Light rose shaded region indicates the deficit in CDI expected for a expression ratio corresponding to heterozygous mutation in *CALM2* gene, while dark rose shaded region indicates predicted extent of CDI reduction for homozygous mutation.

C, Exemplar current traces with the colors corresponding to the Langmuir plot in **B**. For each set of records, the Ca^{2+} trace is the lighter color waveform, and the corresponding Ba^{2+} trace is normalized to the peak of the Ca^{2+} trace for comparison of decay kinetics. Scale bar corresponds to Ca^{2+}. Exemplar traces on far right are from a cell expressing CaM_{WT} only ($\hat{\gamma} = \infty$), as reproduced from Figure 2A for reference.

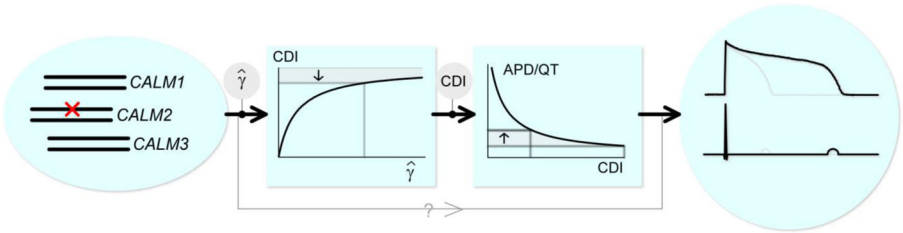

Figure 7. Proposed mechanism of electrical and calcium dysfunction for LQTS CaM mutants

Flow diagram schematizing how heterozygous *CALM2* mutation might lead to fractional decrease in CDI, yielding action potential prolongation and ultimately long QT phenomena.

Table 1

Average values for APs recorded at 0.5 Hz pacing

CaM	APD_{80} (ms)	$(dV/dt)_{max}$ (mV/ms)	V_{rest} (mV)**	V_{max} (mV)
WT	417.0 ± 6	119.9 ± 3.2	−62.0 ± 0.2	55.7 ± 0.4
D130G	824.2 ± 16*	112.5 ± 2.1	−61.3 ± 0.2	48.4 ± 0.6
D96V	973.6 ± 12*	139.5 ± 1.7	−62.6 ± 0.1	56.3 ± 0.3
F142L	874.8 ± 22*	131.7 ± 3.8	−61.8 ± 0.2	51.8 ± 0.5
N54I	391 ± 4.5	128.7 ± 1.4	−64.9 ± 0.3	53.6 ± 0.3
N98S	751.8 ± 5.8*	160.6 ± 1.0	−62.4 ± 0.1	58.1 ± 0.1

* $P < 0.01$;

** Values consistent with those expected for aGPVMs after one day in culture [56, 57].